Controlled Growth of 3R Phase Tantalum Diselenide and Its Enhanced Superconductivity

Ya Deng[1,†], Yuanming Lai [2,†], Xiaoxu Zhao[3,†], Xiaowei Wang[1], Chao Zhu[1], Ke Huang[2], Chao Zhu[1], Jiadong Zhou[1], Qingsheng Zeng[1], Ruihuan Duan[1], Qundong Fu[1], Stephen J Pennycook[3,*], X. Renshaw Wang [2,*], Zheng Liu[1,*]

[1] Center for Programmable Materials, School of Materials Science & Engineering, Nanyang Technological University, Singapore 639798, Singapore

[2] School of Physical and Mathematical Sciences & School of Electrical and Electronic Engineering, Nanyang Technological University, 639798 Singapore

[3] Department of Materials Science and Engineering, National University of Singapore, Singapore 117575, Singapore

[†]These authors contributed equally to this work.

*Corresponding author: z.liu@ntu.edu.sg; renshaw@ntu.edu.sg

Abstract

Layered transition metal dichalcogenides (TMDs), bursting with numerous possibilities endowed by the combinations of not only a large variety of compounds, but also rich crystal structures. Exploring new materials, identifying their structures and properties have always been the original motivation in materials science. Here, we report the synthesis and enchanted superconductivity of rare $TaSe_2$ with three-layer stacking sequence (3R). An ambient pressure chemical vapor deposition (CVD) strategy has been used to achieve pure 3R-$TaSe_2$. Low-temperature transport data reveals a high superconducting transition temperature (T_c) of 1.6 K in the 3R-$TaSe_2$, which is significantly higher than that of the two-layer stacking sequence (2H, H: hexagonal) phase. The results reveal that the T_c is rather sensitive to the layer-stacking order, and confirm that 3R is strongly preferred for superconductivity over the2H in the $TaSe_2$. This work demonstrates the synthesis of a unique 3R phase platform to study superconducting properties and provides fresh insights on manipulating crystal structures to gain access to ultra-high T_c.

Introduction

The structure and superconducting properties of 3R TaSe2 have been reported in this work.

Layered transition metal dichalcogenides (TMDs), bursting with numerous possibilities endowed by the combinations of not only a wide variety of materials, but also different crystal structures, have attracted a plenty of attentions. To date, considerable efforts have been paid onto polymorphism of each TMDs, leading to a series of unusual various other charge-ordered states like superconductivity, charge-density-wave (CDW). Among various TMDs, $TaSe_2$ has triggered great attentions due to the high polymorphism of this miraculous material. Meanwhile, the competition and coexistence of superconductivity and CDW-ordered states observed in this material also spark immense focus.

In all crystal structures of $TaSe_2$, the 2H and 1T, due to their intrigue properties, have been extensively studied. For 2H-$TaSe_2$, the two-step CDW transition with incommensurate and commensurate lattice deformations were respectively observed at T = 120 and 90 K, while the temperatures shifted higher to T = 600 K and 473 K for 1T-$TaSe_2$. Both two structures are followed by a superconducting transition at rather low temperature ($T_c \sim 0.2$ K).

Another very interesting structure named 3R was also discovered in the polymorphic $TaSe_2$. The 3R is a structure similar to 2H except for a small, but non-negligible, difference in stacking order of layers, which may result in some novel properties. Recently, 3R molybdenum disulfide and MoS_2 have been synthesized with revealed potentials in applications like nonlinear optics and valleytronics. But for 3R-$TaSe_2$,

basically no studies have been addressed to date. This is partially because the synthesis of pure 3R $TaSe_2$ is an extremely big challenge, as the conventional chemical vapor transport (CVT) method generally results in a mixture of 2H and 3R phases in products. In contrast, the chemical vapor deposition (CVD) approach is inherently superior in synthesis of pure 3R $TaSe_2$ as it allows a more flexible control of growth parameters, which makes itself a good platform to experimentally synthesize 3R $TaSe_2$.

Here we report an ambient pressure CVD strategy to synthesize 3R-$TaSe_2$. The morphologies, chemical composition and crystal quality of products have been investigated by a series of characterizations such as optical microscopy, atomic force microscopy, Raman and X-ray photoemission spectroscopy (XPS). The results indicate the high crystallinity and uniform morphology of $TaSe_2$. Then, the atomic resolution scanning transmission electron microscopy (STEM) has precisely confirmed the 3R stacking structure of as-synthesized $TaSe_2$. Low-temperature transport data reveals a high T_c of 1.6 K in the 3R-$TaSe_2$, which is an order of magnitude higher than that of 2H phase. The results are in consistent with the results of Ta-containing ternary compounds, however, as the effects of doping are excluded here, they serve as the first direct evidence that the 3R stacking order is indeed the origin of higher T_c.

Synthesis and characterization of TaSe2 atomic layers.

Atomically thin TaSe2 crystals were grown on SiO2/Si substrate through ambient pressure CVD process. The experiment setup is shown in Supplementary Figure S1. The mixed compounds of Ta and $TaCl_5$ with a ratio of 10:1 were placed at the center of tube furnace. The SiO2/Si substrate was suspended on the ceramic boat as shown in Figure S1. This structure allows the precursor to be close to the substrate and on which more products can be deposited. The Se powder was placed upstream. The carrier gas ratios of Ar and H2 were set as 32:8 for a relatively high nucleation density (Fig. S2). Then the TaSe2 crystals can be obtained on the polished surface of SiO2/Si substrate. The key to successfully synthesis TaSe2 atomic layers depends on the selection of suitable source materials and the careful regulation of growth process. Experiments details and possible growth mechanism are provided in the “Methods” section and Supplementary Figure S1.

Figure 1a exhibits a structure model of monolayer 1H-phase TaSe2. According to previous reports, the CDW materials of TaSe2 mainly has three kinds of lattice structures, namely 1T, 2H and 3R, and their structures are shown in **Supplementary Table 1,** which are not described here. For monolayer TaSe2, no matter the bulk crystal is 2H or 3R phase, it is the same 1H structure (Fig. 1a). Due to the structure similarities of 2H and 3R TaSe2, there is basically no difference in morphologies.[1] The optical microscopy and scanning electron microscopy (SEM) have been used to characterize as-synthesized TaSe2 crystals. The TaSe2 atomic layers on SiO2/Si substrate generally present triangular shapes (Fig. 1b-f). Almost no cracks and impurities can be seen form monolayer TaSe2 surface (Fig. 1b). Atomic force microscope (AFM) height measurements indicate the thickness of as-grown monolayer TaSe2 is near 1.4 nm. The following Scanning Electron Microscope (SEM) image further confirms the high

quality of produced TaSe2 crystals (Fig. 1d). The representative morphologies of TaSe2 crystals with different thickness are shown in Fig. 1e-f, where Bilayer (2L), and bulk TaSe2 are clearly distinguished by color contrast. The optical images also show the size of as-grown TaSe2 exceeding 100 μm.

Raman spectroscopy under laser excitation wavelength at 514 nm is performed to characterize the lattice vibrational modes of the synthesized TaSe2. The typical Raman spectra of synthesized TaSe2 crystals with different thickness are shown in Fig. 1g. The Raman spectra, of 2H TaSe2 have been referred directly, because the 2H and 3R structure differences are very small, making their Raman characterics basically no difference, which is confirmed in the MoS2. Two dominant Raman-active modes at 232 and 217 cm^{-1} are observed in monolayer TaSe2, which are corresponding to A_{1g} and E_{2g} symmetries respectively. The namely A_{1g} and E_{2g} modes in TaSe2 arises from out-of-plane and in-plane vibration. For the broaden peaks around 140 cm^{-1}, contributed to the broad second-order peak (~141) and E1g mode (~138 cm^{-1}), is no longer unfolded (discuss in detail) here.Then we focus on the A_{1g} and E_{2g} modes. The red-shift of the E_{2g} peak and blue-shift of A_{1g} peak can be obviously observed from monolayer to bulk TaSe2. To further analyze the relationship between Raman features and the number of layers, the Lorentz function was used to fit the A1g and E2g peaks. The fitting results are plotted in **Supplementary Figure S3**. It can be observed that with the decreasing number of layers, the peak position of E2g decreases while A1g increases. A maximum shift of 7.4 cm for E2g peak can be obtained from the comparison of monolayer and bulk TaSe2. These shifts all can be attributed to the structure changes of TaSe2 with different thickness, essentially caused by the interlayer Van der Waals force or long-range coulom bic interlayer interactions. The layer-dependent Raman feature observed in TaSe2 is similar to that of MoS2. It means the layer-dependent Raman spectra of TaSe2 also can be used to identify the layer number like MoS2. Figure 1h show a representative Raman mapping image of triangular TaSe2 atomic layers at the intensity of A1g modes. The color contrasts are uniform across the whole triangular shape, indicating the high-quality aspect of the TaSe2 crystal. Furthermore, the micro-spot X-ray photoemission spectroscopy (XPS) was employed to analyze the chemical composition of the synthesized materials. As shown in Figure S4, the observed XPS spectra of the Ta 4f and Se 3d photoelectric peaks matched well with Ta^{4+} $4f_{7/2}$, Ta^{4+} $4f_{5/2}$, Se^{2-} $3d_{5/2}$ and Se^{2-} $3d_{3/2}$ respectively, which are agreement with the reported spectra of TaSe2. The Ta:Se atomic ratio calculated from the XPS data is close to 1:2, confirming the formation of stoichiometric TaSe2.

Structural characterization of 3R phase TaSe2

To further check the crystal quality and more importantly verify the stacking order of the as-synthesize sample, spherical aberration-corrected STEM (Cs-corrected STEM) has been employed to observe the lattice fringes. The polymorphism of the CVD grown $TaSe_2$ is unveiled by atomic resolution scanning transmission electron microscopy – annular dark field (STEM-ADF) imaging. The STEM-ADF imaging was widely applied for disclosing the polymorphs and stacking

polytypes in 2D materials as the image contrast is directly related to the atomic number Z. [ref1-2] The STEM image of a monolayer $TaSe_2$ film (Fig. 2a) reveals a signature honeycomb structure suggesting that the as-grown $TaSe_2$ is H-phase [ref2] which is further verified by the image simulation (Fig. 2b). Unlike frequently observed chalcogen vacancies in group VIB transition metal dichalcogenide monolayers (TMDCs) [ref3], we constantly observed metal (Ta) vacancies in monolayer $TaSe_2$ as depicted Supplementary Figure 4 presumably ascribed to a relative lower formation energy. [ref4] In addition, the topological edges in $TaSe_2$ terminating along the zigzag direction is not atomically sharp, instead we found a ~ 1 nm thin layer of amorphous region decorated along the edge region as highlighted in Fig. 2c. The amorphous edge was presumably due to the oxidation during the sample transfer. The energy-dispersive X-ray spectroscopy (EDS) mapping shown in Fig. 2d revealing the uniform dispersion of Ta and Se elements in whole TaSe2 flakes. Meanwhile, the chemical stoichiometry of the as-grown $TaSe_2$ was confirmed a 1:2 ratio by the EDS spectrum (Supplementary Figure 5a), which is consistent with the previous XPS result. The presence of Ta and Se species was further verified by the electron energy loss (EEL) spectroscopy (Supplementary Figure 5b) where sharp Ta-O edge and Se-M edge were clearly seen.

The stacking polytype in multilayer film offers another degree of freedom to modify a wide range of properties in 2D materials. [ref1, ref5] In the CVD grown multilayer $TaSe_2$, we noticed that the stacking polytype consistently complies a 3R-stacked configuration regardless of the layer number. Apparently, a bilayer and trilayer 3R-stacked $TaSe_2$ film were depicted in Fig. 3a, and Fig. 3e, respectively. Unlike an eclipsed configuration in 2H-stacked TMDs, 3R stacking order takes a staggered configuration and additional atoms blobs appears in the centre of each honeycomb as shown in the enlarged STEM images of bilayer (Fig. 2b) and trilayer (Fig. 3f) $TaSe_2$ films. [ref1] Corresponding simulated image (Fig. 3c, and Fig. 3g) greatly resembles the experimental images (Fig. 3b, and Fig. 3f) in both films suggesting a 3R stacking order widely exist in multilayer $TaSe_2$ crystals. Single set of spots were observed in fast Fourier transform pattern of bilayer (Fig. 3d) and trilayer (Fig. 3h) films, and limited point defects or line defects were found suggesting the CVD grown $TaSe_2$ crystal is highly crystalline.

Superconductivity in 3R phase TaSe2

It is well-known that the physical properties of layered materials are generally very sensitive to the difference in crystal structures, especially the phase structure. However, compared to the other two phases, the physical properties of 3R TaSe2 have been rarely addressed. In what way is the electrical property of 3R phase different from 1T and 2H phases in TaSe2? Would the 3R phase outperform others in quality of electrical transport? To answer these questions, the low-temperature transport experiments were performed to characterize the electrical properties of synthesized 3R-TaSe2. First, we fabricated the Hall-bar device by using standard electron beam lithography (EBL) process (see “Methods” section). The optical image and schematic diagram of device

are shown in Fig. 4a. For a better demonstration of device structure, in the inset of Fig. 4a the multilayer 3R-TaSe2 used in device is simplified into a single layer. The normalized resistance R(T)/R(T=300 K) versus temperature is plotted in Fig. 4b. As reported in previous work, the phase transition in TaSe2 reveals itself through the change in the slope of temperature-resistance curve.

In the figure a featured phase transition could be observed at the resistance of 3R-TaSe2 at 90 K, which may be attributed to the commensurate charge density wave (CCDW) transition. Note that this signature is relatively weaker than those reported in 2H- or 1T-TaSe2. Nevertheless, what makes it astonishing is the low-temperature transport data shown in the inset of Fig. 4b. The resistance begins to decrease once the temperature is below a critical transition temperature Tc of 1.6 K (defined as the temperature corresponding to 90% normal state resistance) and drops to zero at 0.5 K, revealing the existence of superconductivity at a significantly higher temperature than the critical temperature in other phases of TaSe2 (Tc ~ 0.2 K).

Figure 4c displays the dependence of resistance on temperature obtained at different magnetic field at low temperatures. We can see the T_c decrease at larger external magnetic field and the superconductivity is completely suppressed when the magnetic field reaches 1.00 T. This is because the perpendicular external magnetic field may cause vortices, leading to dissipation and inhibition of superconductivity[8].

Figure 4d shows the current–voltage (*I–V*) characteristics of TaSe2 with a variety of temperatures. The presence of zero-resistance further proves the existence of superconducting states. These results support the characteristics of resistance observed in Fig. 4b and 4c. In addition, the *I-V* characteristics (the inset in Fig. 4d) show a significant critical current I_c, which pins at zero until the temperature is above 1.8 K. It is clear that the critical current I_c provides a convincing evidence for high T_c superconductivity. The temperature dependent upper critical field B_{c2} is extracted from the resistance curves in **Fig. S** and marked as red squares at separated magnetic fields in Fig. 4e. Then, the data was fitted based on standard Ginzburg–Landau theory[8–10]: $B_c = [\frac{\Phi_0}{2\pi\xi_{GL}^2}](1-\frac{T}{T_c})$, where Φ_0 is the flux quantum and equal to h/2e, ξ_{GL} is the Ginzburg–Landau superconducting coherence length. The linear behavior of fit line is usually regarded as the characteristics of 2D superconductors. The coherence length (ξ_{GL}) derived from the fitting of B_c is about 85 nm at T = 0 K. Figure 4f displays the differential resistance dV/dI as a function of current I for different temperatures. Below 0.6 K with a small current bias, the sample reveals a zero-resistance state, which corresponds to superconductivity. With low current bias, the differential resistance shows a downward trend within a range of temperature between 0.8K and 1.6K, indicating that the superconducting residual rather than the zero-resistance state[11]. Superconductivity disappears when the temperature is beyond 1.8 K. Similar results were also obtained and presented through *I–V* characteristics and differential resistance (Figure S7). These results further confirm that 3R-$TaSe_2$ has superconductivity with a critical temperature T_c above 1.6 K.

As one of the signatures of 2D superconductors, a linear fitting behavior is observed in Fig. 4c. The 2D superconductor generally refers to (one category of) film-like material

whose superconductivity is considered to be confined in two dimensions. In this type of superconductor, the Berezinskii-Kosterlitz-Thouless (BKT) transition has been intensively studied and regarded as the evidence of 2D superconductivity. Similarity, we study the BKT transition in TaSe2 to confirm the 2D nature of its superconductivity for a deeper understanding of its superconducting properties. Figure 5a shows the logarithmic-scale Voltage-Current (*V-I*) data with different temperatures. The power-law dependence ($V \propto I^{\alpha}$) has been used to fit the behavior of *V-I* curve, with the results are shown as short black line. As is well-known, the BKT temperature, defined as the temperature where the $V \propto I^3$ behavior is satisfied, plays a very important role in BKT transition. In Fig. 5a, the left solid black lines correspond to an Ohmic behavior ($V \propto I$) while the long solid violet line refers to $V \propto I^3$ behavior in the range from 0.8 K to 1.0 K, indicating the variation interval of $\boldsymbol{T_{BKT}}$ has been preliminarily confirmed In Fig. 5b presented are the exponential α derived from the slopes of short black lines in Fig. 5a. The intersection indicated by the black arrow shows an estimated T_{BKT} of 0.94 K. Overall these results confirm our 3R-TaSe2 material as a quasi-2D superconductor with a Tc of 1.6 K and T_{BKT} of 0.94 K.

As discussed above, our results indicate the 3R-TaSe2 material is provided with a relatively weak signature of CCDW transition at 90 K and a high superconductivity transition temperature Tc of 1.6 K. This is in stark contrast with the electrical properties of other two phases TaSe2 in previous reports, in which the TaSe2 shows a sharp ICDW transition at 120K and a low Tc of 0.2 K. By switching the phase from 2H to 3R in TaSe2, the Tc can be increased by a nearly an order in magnitude. This can be attributed to the suppression of CDW during its competition with superconductivity. This conclusion is highly in consistent with results reported in the pressure-enhanced superconductivity of TaSe2, where a high pressure was applied to the 2H-TaSe2, sharply increasing the Tc while simultaneously decreasing the T_{cdw}. In our work, a high Tc could be obtained straightforward in a 3R-TaSe2 with no requirement of high pressure. This result is supported by the work on different phase structures of Ta-containing ternary compounds. By excluding the effect of doping, the 3R stacking order is confirmed as the origin of higher Tc.

In summary, for the first time, we have synthesized the pure 3R-$TaSe_2$ through the CVD method. The 3R stacking structure of as-synthesized $TaSe_2$ has been rigorously confirmed by the atomic resolution STEM. As signatures of electrical properties of 3R-$TaSe_2$, a high T_c of 1.6 K, along with a relatively weak CDW transition have been observed. This phenomenon is well consistent with the previous reports on enhancement of superconductivity caused by the pressure or structural changes. The increase of T_c might be attributed to a consequence of phonon hardening or the structure induced changes in Fermi-surface. Our work serves as the first direct evidence that the 3R stacking order is indeed the origin of higher T_c in $TaSe_2$. More importantly, it provides fresh insights on manipulating crystal structures to gain access to ultra-high Tc.

Figures

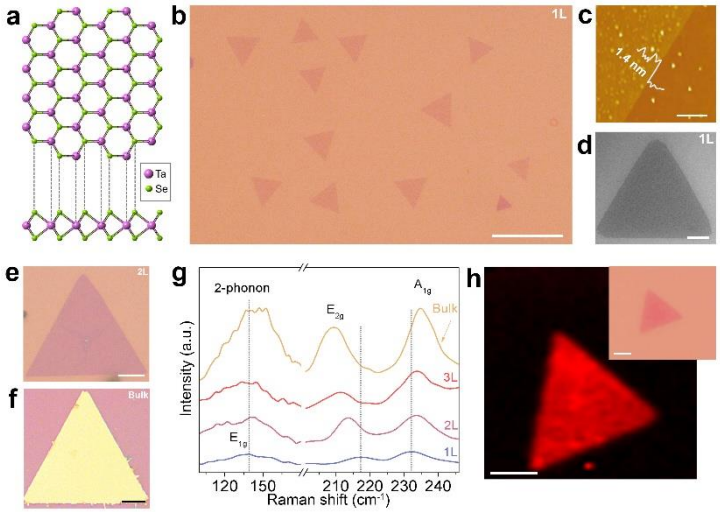

Fig. 1 Synthesis and characterization of $TaSe_2$ atomic layers on SiO_2/Si substrates. (a) Atomic structure of monolayer (1L) 1H-$TaSe_2$ viewed from top-down and side directions. (b-d) Representative optical (b), AFM (c) and SEM (d) images of monolayer $TaSe_2$ single crystals. (e-f) Representative optical images of bilayer (2L) and bulk $TaSe_2$. (g) Typical Raman spectra of synthesized $TaSe_2$ crystals with different thicknesses. The dashed lines are for eye guidance. Obvious shifts can be seen form the spectra comparison. (h) Raman intensity mapping (A_{1g} mode) of as-grown triangular $TaSe_2$ atomic layers from the region of inset. The scale bars are 20 μm in b, e, f and 2 μm in c, d, h.

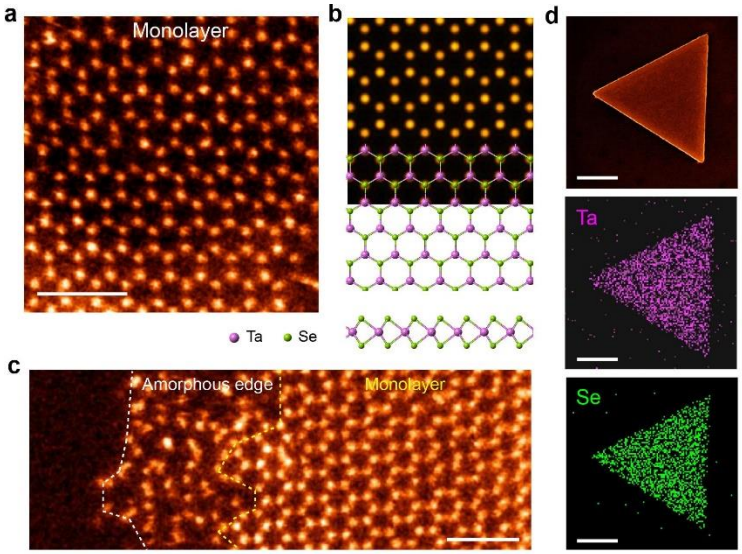

Fig. 2 Atomic structures of monolayer H-phase $TaSe_2$. (a) An atomic resolution STEM-ADF image of a monolayer H-phase $TaSe_2$. (b) Corresponding simulated image overlaid with the atomic model. (c) STEM-ADF image showing a thin layer of amorphous edge in a monolayer H-phase $TaSe_2$. (d) SEM image and corresponding Energy-dispersive X-ray spectroscopy (EDS) elements mapping of as-grown triangular $TaSe_2$ flakes. Scale bars: 1 nm.

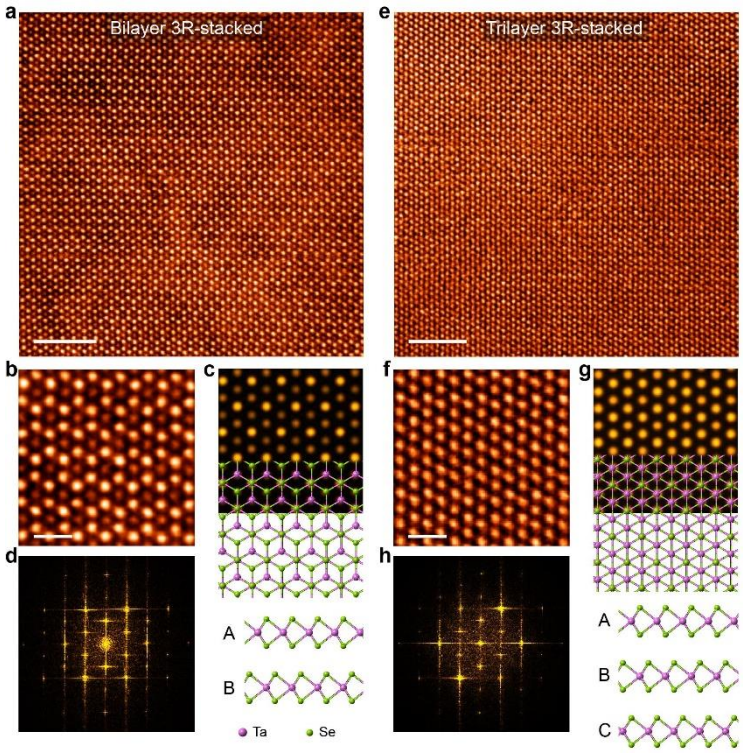

Fig. 3 3R stacking polytypes in few-layer H-phase $TaSe_2$. (b) Atomic resolution STEM-ADF image showing a bilayer 3R-stacked $TaSe_2$ film. (b) Enlarged image from a and (c) its simulated image overlaid with the atomic model. The side view was depicted in the lower panel. (d) Fast Fourier transform (FFT) pattern of a. (e) Atomic resolution STEM-ADF image showing a trilayer 3R-stacked $TaSe_2$ film. (f) Enlarged image from a and (g) its simulated image overlaid with the atomic model. The side view was depicted in the lower panel. (h) FFT pattern of e. Scale bars: 5 nm in (a, e); 0.5 nm in (b, f).

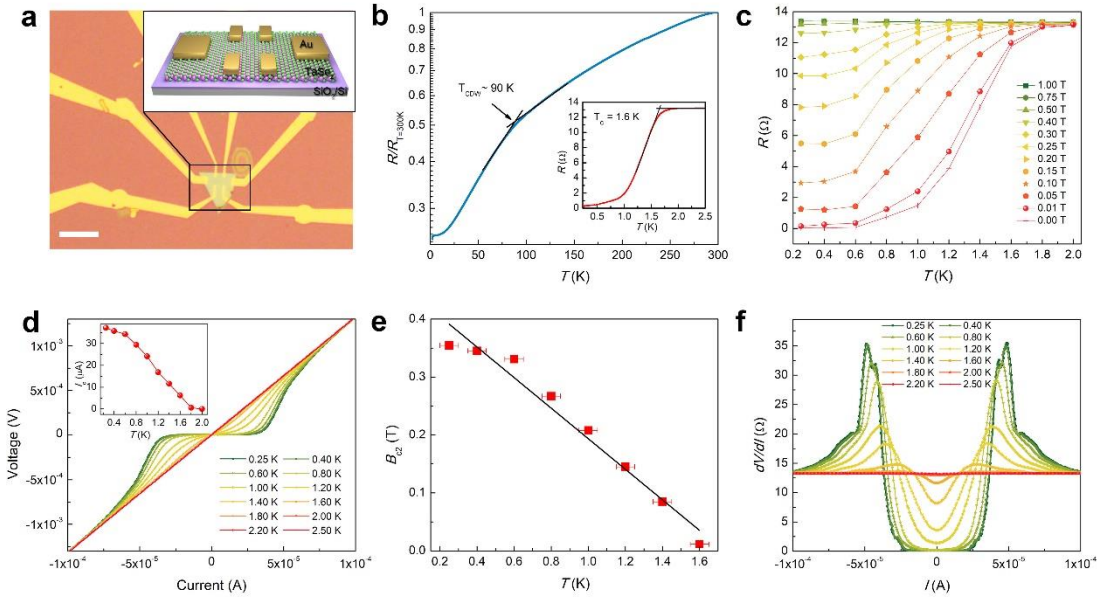

Fig. 4 Low-temperature transport properties of synthesized 3R-$TaSe_2$. (a) Optical image and schematic

structure (inset) of 3R-$TaSe_2$ Hall-bar device. The scale bar is 20 μm (b) The temperature dependence of normalized resistance R(T)/R(T=300 K). The inset shows a superconducting critical temperature, T_c, of 1.6 K. (c) Temperature-dependent resistance measured under different magnetic fields. (d) Current-dependent voltage at different temperatures. The inset is the temperature-dependent critical current (I_c). (e) The upper critical field (B_{c2}) as a function of temperature. The solid line in the inset is the linear fit to the data based on the Ginzburg-Landau theory. The error bars represent the range of rounding region of the transition near R=0. (f) A typical differential resistance dV/dI as a function of current at different temperatures.

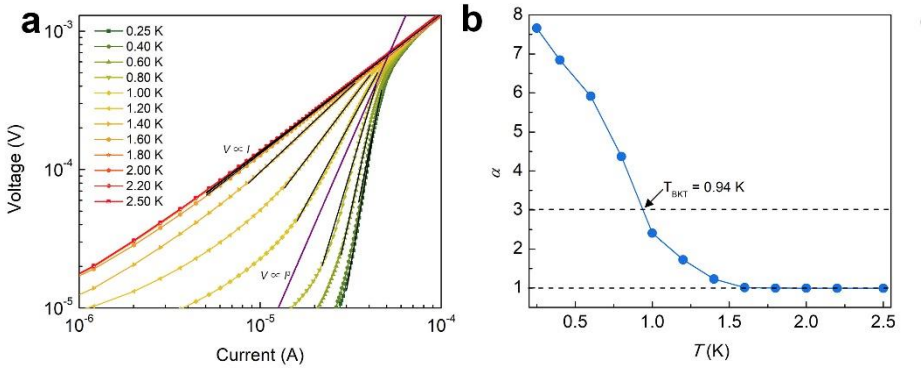

Fig. 5 BKT transition in 3R-$TaSe_2$. (a) The voltage-current data plotted in a logarithmic scale at different temperatures. The solid black lines correspond to an Ohmic behavior ($V \propto I$), while the long solid violet line corresponds to $V \propto I^3$ behavior at the BKT transition in the range from 0.8 to 1.0 K. (b) The temperature dependence of the exponent α deduced by fitting the data in (a) via power-law theory. The intersection indicated by the black arrow shows the T_{BKT} is 0.94 K as α crosses 3.

Methods

CVD growth of TaSe2 crystals

As shown in supplementary Fig 1, The precursors of Se powder (1g) and mixed Ta/$TaCl_5$ powders (10 mg/1 mg) were placed upstream and at the center of a one-inch quartz tube respectively. The alumina boats were used to hold the powers, as usually did in conventional CVD setup. The SiO2/Si substrate was suspended on the ceramic boat so that the products can be deposited on it. The 32 sccm Ar and 8 sccm H2 were used as the carrier gases. The furnace was heated up to 800 ° C within 18 minutes and held at which for 12 minutes. Afterwards the furnace was naturally cooled to 600 ° C with the same carrier gas. The top cover was finally opened to quickly cool the sample and the carrier gas was switched to 100 sccm Ar.

Device fabrication and transport measurement

The Si substrates with 300 SiO_2 were used to deposit the 3R-TaSe2 flakes directly to avoiding additional transfer process for transport measurements. Then the standard e-beam lithography (EBL) was used to fabricate Hall-bar devices. Next, the contact Ti/Au electrodes with a

thickness of 5/50 nm were deposited on the sample using an electron-beam evaporator. After the lift-off process in acetone, the TaSe2 based devices were fabricated. The magnetic transport experiments were measured through Oxford Instruments. The measuring temperature was cooled down to 0.25 K to obtain the superconducting transition temperature of TaSe2. The resistance values were collected by Keithley 6221 and 2182 source meter. To reduce the thermal effect, a small current (1μA) was used to perform the transport test.

Reference

Acknowledgements

X.R.W. acknowledges supports from the Nanyang Assistant Professorship grant from Nanyang Technological University and Academic Research Fund Tier 1 (RG108/17 and RG177/18) and Tier 3 (MOE2018-T3-1-002) from Singapore Ministry of Education.

Author contributions

Supporting Information

Discussion of the growth mechanism

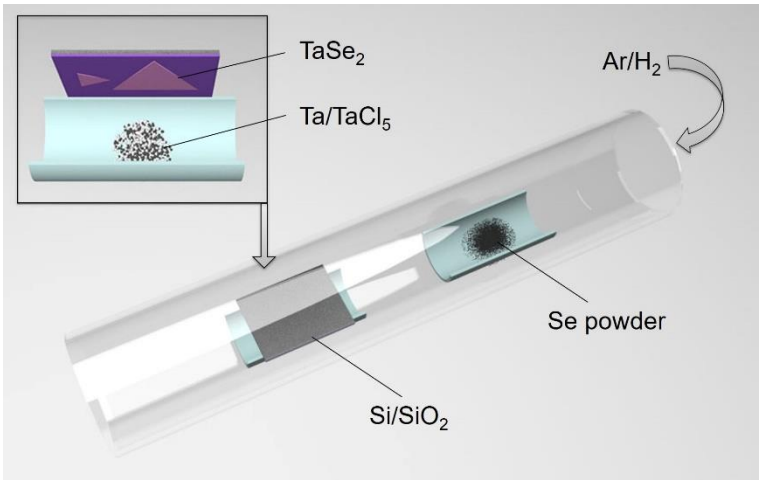

Figure S1. Schematic of the reaction chamber for the controlled synthesis of TaSe2 atomic layers

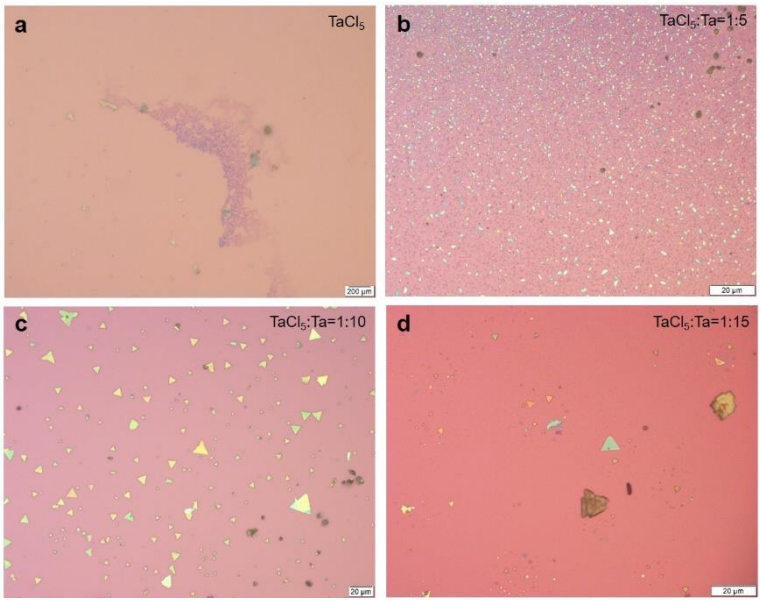

Figure S2. Typical optical images of synthesized $TaSe_2$ flakes using precursors of $TaCl_5$ and Ta with different weight ratio.

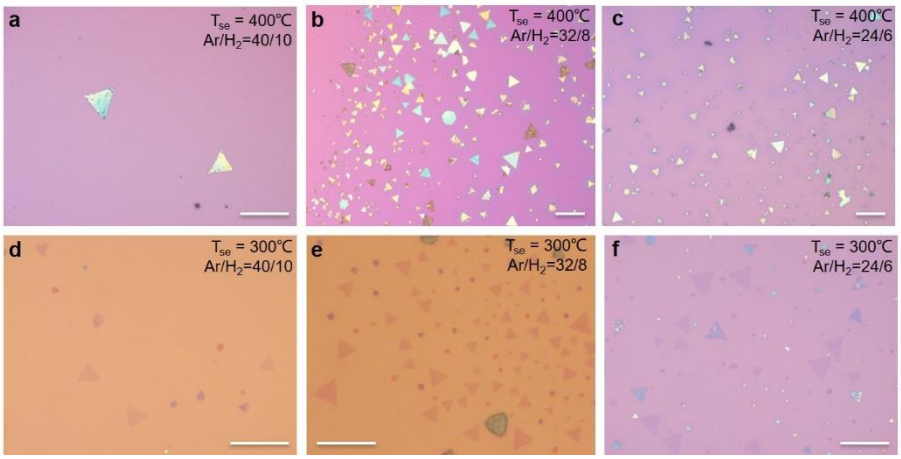

Figure S3 The optical images of TaSe2 flakes synthesized with alternating flow of the carrier gas (sccm) and temperature of Se precursor (T_{Se}). Higher or lower flow rate of carrier gas will reduce the nucleation density, while higher T_{Se} will result in the thicker flakes. This T_{Se} dependent phenomenon is consistent with the previous reported NbSe2 material. The scale bars are 20 μm. The unit of flow is sccm.

Discussion of possible growth mechanism

As the TaSe2 crystals grown before is mainly through Chemical Vapor Transport (CVT) method, which produce the bulk crystals. However, as the structures of 2H and 3R are very similar, the produced 3R TaSe2 is often a mixture of two phases. Different from the synthesis of 1T phase, the 2H and 3R phase are difficult to distinguish by control the growth parameter. Until now, there is not any report on the synthesis of 3R phase TaSe2 single crystals.

In our experiment, we first synthesized the 3R phase TaSe2 by the Chemical Vapor Deposition (CVD) method. The CVD has been demonstrated as a facile method in synthesizing atomic thin crystals in large scale (jd). Thinner products, more precise control, make CVD method

easier to obtain pure 3R phase TaSe2, compared to the CVT method. For the synthesis of 3R TaSe2, the method is second, the appropriate precursor and precise synthesis process control are the most critical. It has been reported that chloride can facilitate the synthesis of 3R phase 2d materials due to lowering the melting point of the chemicals.[2] However, if only using TaCl5 as the sources, the reaction is too rapid to be controlled (figure S2a). Based on the CVD synthesis experiences of our group (WH,and JD), we use the optimized CVD method to synthesize the 3R TaSe2. After a series of CVD experiments, the precursor of mixed compounds (Ta:$TaCl_5$=10:1) and optimized carrier gas ratio (Ar/H_2=32/8) are used and proved to be suitable (Figure S2 and S3). The growth temperature was carefully optimized at 800°C to avoid the 1T phase formation under high temperature.

Table S1. The top views of the crystal structure of $TaSe_2$. The purple and green spheres represent Ta and Se atoms, respectively.

Thickness / Phase	Monolayer	Bilayer	Trilayer and above
1T		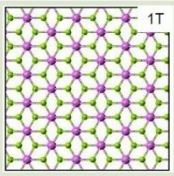	
2H	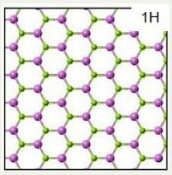	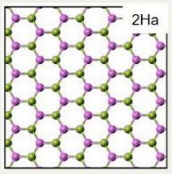	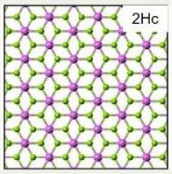
3R		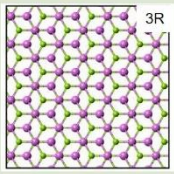	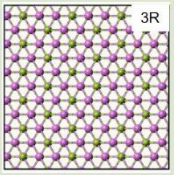

The TaSe2 has mainly three kinds of lattice structures, namely 1T, 2H and 3R, and their structures are shown above. **For 1T $TaSe_2$, the top views of crystal structures with different thickness are always similar, as shown in the inset of first row.** For monolayer $TaSe_2$, no matter the bulk crystal is 2H or 3R phase, it is the same 1H structure.

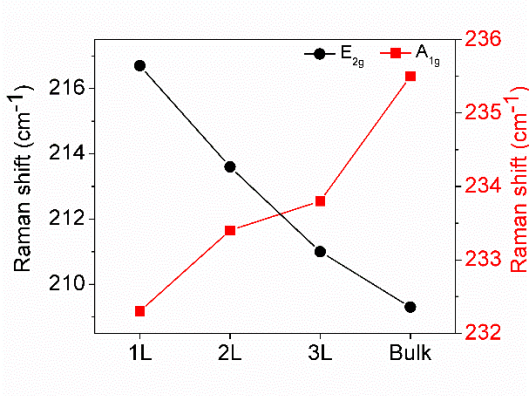

Figure S3. Raman peak position of $TaSe_2$ plotted as a function of the thickness.

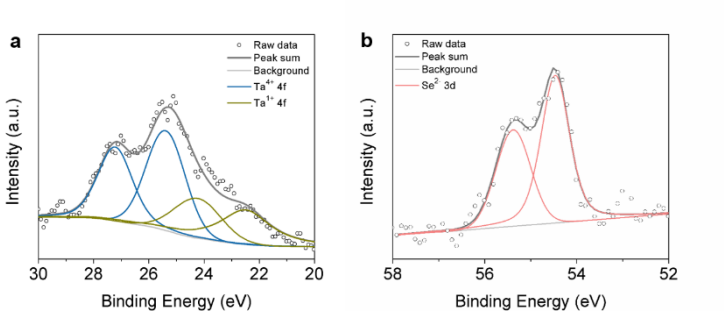

Figure S4. X-ray photoemission spectroscopy (XPS) spectra of the Ta 4f and Se 3d peaks from the synthesized $TaSe_2$ flakes. The size of analysis area was set to 15μm so that the data can be only collected from one single-crystal $TaSe_2$. The main Ta 4f and Se 3d core-levels spectra can be fitted with Ta^{4+} $4f_{7/2}$, Ta^{4+} $4f_{5/2}$, Se^{2-} $3d_{5/2}$ and Se^{2-} $3d_{3/2}$ respectively, which are agreement with the reported spectra of TaSe2. The Ta:Se atomic ratio calculated from the XPS data is close to 1:2, confirming the formation of stoichiometric TaSe2. The peaks marked with green line in **a** can be attributed to the binding energy of the Ta^{1+} state. Which is speculated to come from the surface oxide of Ta_2O due to the inevitably exposed to the air when prepare the XPS samples.

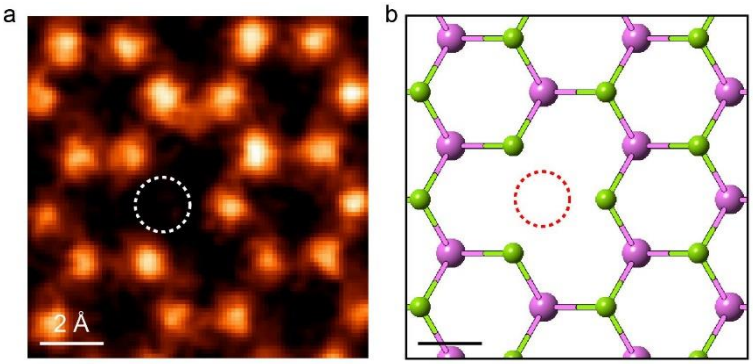

Figure S4. (a) An atomic resolution STEM-ADF image showing the presence of a Ta vacancy in a monolayer $TaSe_2$ film and (b) its corresponding atomic model.

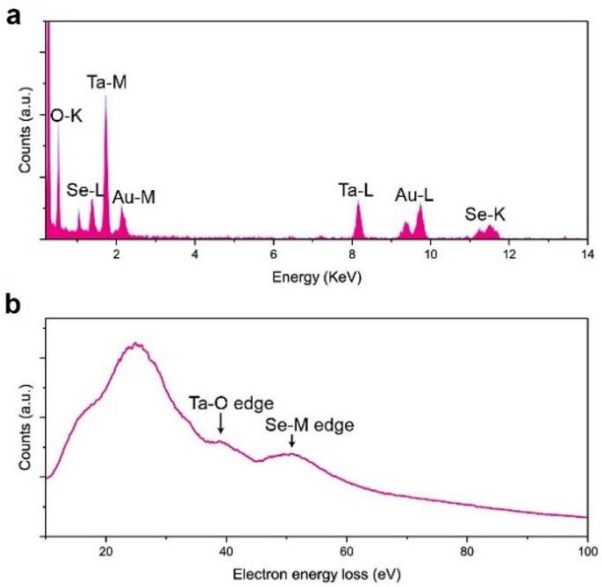

Figure S5. (a) Energy-dispersive X-ray spectroscopy (EDS) and (b) electron energy loss (EEL) spectrum of the as-grown $TaSe_2$ films.

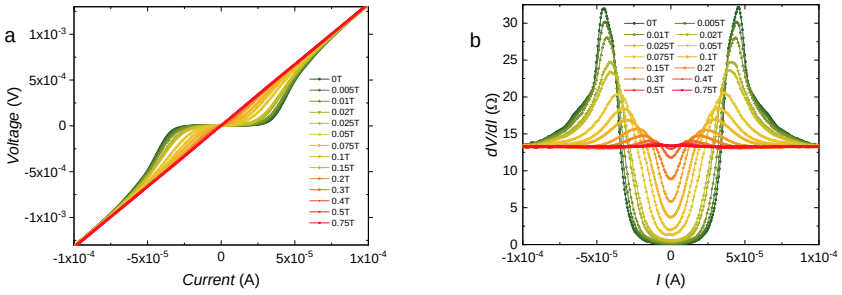

Figure S7. The superconducting properties of 3R-$TaSe_2$ at 0.6 K. (a) Current-voltage (I-V) characteristics with different magnetic field. (b) A typical differential resistance dV/dI as a function of current for different magnetic field.

1. Samnakay R, Wickramaratne D, Pope TR, Lake RK, Salguero TT, Balandin AA. Zone-Folded Phonons and the Commensurate–Incommensurate Charge-Density-Wave Transition in 1T-TaSe2 Thin Films. *Nano Lett* **15**, 2965-2973 (2015).